RAA 2015 Vol. **15** No. **5**, 753–763 doi: 10.1088/1674–4527/15/5/012
http://www.raa-journal.org *http://www.iop.org/journals/raa*

Research in Astronomy and Astrophysics

Electron content near the lunar surface using dual-frequency VLBI tracking data in a single lunar orbiter mission

Zhen Wang[1,2], Na Wang[1] and Jin-Song Ping[2]

[1] Key Laboratory of Radio Astronomy, Xinjiang Astronomical Observatory, Chinese Academy of Sciences, Urumqi 830011, China; *wangzh@xao.ac.cn*

[2] Key Laboratory of Lunar and Deep Space Exploration, National Astronomical Observatories, Chinese Academy of Sciences, Beijing 100012, China; *jsping@bao.ac.cn*

Received 2014 June 30; accepted 2014 September 6

Abstract In VLBI observations of *Vstar*, a subsatellite of the Japanese lunar mission *SELENE*, there were opportunities for lunar grazing occultation when *Vstar* was very close to the limb of the Moon. This kind of chance made it possible to probe the thin plasma layer above the Moon's surface as a meaningful by-product of VLBI, by using the radio occultation method with coherent radio waves from the S/X bands. The dual-frequency measurements were carried out at Earth-based VLBI stations. In the line-of-sight direction between the satellite and the ground-based tracking station where VLBI measurements were made, the effects of the terrestrial ionosphere, interplanetary plasma and the thin lunar ionosphere mixed together in the combined observables of dual-frequency Doppler shift and phase shift. To separate the variation of the ionospheric total electron content (TEC) near the surface of the Moon from the mixed signal, the influences of the terrestrial ionosphere and interplanetary plasma have been removed by using an extrapolation method based on a short-term trend. The lunar TEC is estimated from the dual-frequency observation for *Vstar* from UT 22:18 to UT 22:20 on 2008 June 28 at several tracking stations. The TEC results obtained from VLBI sites are identical, however, they are not as remarkable as the result obtained at the Usuda deep space tracking station.

Key words: planets and satellites: atmospheres — occultations — detection

1 INTRODUCTION

Predecessors in the field of lunar ionosphere research have already done a large amount of interesting investigations, among which one result suggested the existence of a lunar ionosphere. In the 1960s, refraction of radio waves transmitted from Quasi Stellar Objects was observed during a lunar occultation event (Andrew et al. 1964). Under certain conditions for solar wind plasma and cosmic rays, the number density of photoelectrons at a height of a few hundred meters on the hemisphere with lunar dayside was estimated to be on the order of $10^4\ \mathrm{cm}^{-3}$ (Walbridge 1973). Using the technique of radio occultation with a single satellite and assuming that an ionosphere has a spherically symmetric distribution around the Moon, the Soviet lunar missions of Luna 19 and Luna 22 detected peaks in ionization density as large as $500 - 1000\ \mathrm{cm}^{-3}$ at heights of 5–10 km above the lunar surface on the sunlit side of the Moon. The electron number densities gradually decreased at a height of 10 km or higher and at 5 km or lower (Vasil'Ev et al. 1974; Vyshlov 1976; Vyshlov et al. 1976; Vyshlov & Savich 1979). Savich (1976) argued that remnant magnetic fields might be shielding the solar wind and allowing plasma to accumulate around the Moon.

Considering that the lunar surface is covered by a thick layer of dust, charged dust particles on the lunar surface could be greatly accelerated by the electric field near the lunar surface and escape from the surface of the Moon, then form wispy floating clouds (Stubbs et al. 2011). Until now, various results have been obtained and suggested by different researchers. Imamura et al. (2012) suggested that electron densities of the order of $100\,\mathrm{cm}^{-3}$ were detected below an altitude of 30 km with solar zenith angles of less than 60°. The extremely high electron density of $500-1000\,\mathrm{cm}^{-3}$ on the surface of the Moon is possibly attributed to human errors in early data processing and analysis (Daily et al. 1977). Without considering the photoelectron sheath layer and solar wind, there cannot be an ionospheric layer around the Moon (Bauer 1996). The ionosphere is distributed from 0 to 100 km in height and is believed to have density on the order of $1\ \mathrm{cm}^{-3}$ (Stern 1999). There are mainly three kinds of generation mechanisms for the thin lunar ionosphere: (1) solar ultraviolet radiation and cosmic rays; (2) a remnant magnetic field around the Moon; (3) charged dust particles from the lunar surface regolith. Until now, the lunar ionosphere, which has a sporadic, tenuous and asymmetric distribution in the vicinity of the lunar surface, has always been a particularly intriguing and controversial subject.

A radio science experiment using the Japanese lunar mission *Selenological and Engineering Explorer* (*SELENE* or *Kaguya*) obtained abundant information on the lunar ionosphere. In addition, this effort provided a new opportunity to detect the morphology and better understand the evolution of the lunar ionosphere, including the radial density distribution, and the effects of diffraction and refraction. At the same time, a regional very long baseline interferometry (VLBI) method was also applied to precisely measure information about the orbit of *SELENE* (Namiki et al. 2009). The raw tracking data on the VLBI observations during the occultation of *SELENE* can be used to retrieve parameters describing the lunar ionosphere. In the following sections, the methods and results related to this project are presented and discussed.

2 SETTING UP THE EXPERIMENT

The *SELENE* lunar mission was successfully launched on 2007 September 14 from the Tanegashima Space Center (Hanada et al. 2010). It consists of three spacecrafts: the three-axis stabilized main orbiter, the relay subsatellite (*Rstar*), and the VLBI subsatellite (*Vstar*), with orbital periods of 120, 240 and 153 minutes, respectively. These three spacecrafts all followed nearly polar orbits. The main orbiter had an average altitude of 100 km around the Moon. The altitudes of *Rstar* and *Vstar* varied from 120 km to 2395 km and from 129 km to 792 km, respectively. In the *SELENE* mission, the VLBI observation (Iwata et al. 2001) used the VLBI Exploration of Radio Astronomy (VERA) network, which consisted of four Japanese telescopes located at Mizusawa (MZ), Iriki (IR), Ishigaki (IS) and Ogasawara (OG) (Kobayashi et al. 2003), and used four additional international telescopes located in Urumqi (UR, China), Shanghai (SH, China), Wettzell (WZ, Germany) and Hobart (HO, Australia) (Schlüter et al. 2002). The baselines ranged from 796 km (SH-IS) to 12 247 km (HO-WZ) (Liu et al. 2010). The VLBI observations were taken with *Rstar* from 2007 October 9 to 2009 February 12 and with *Vstar* from 2007 October 12 to 2009 June 29.

Both subsatellites had the shape of an octagonal prism with size $1\,\mathrm{m}\times1\,\mathrm{m}\times0.65\,\mathrm{m}$. They were covered by solar panels on all sides and weighed approximately 45 kg. Both were also spin-stabilized. The group of dipole antennas used for S- and X-bands onboard the two satellites had medium gain. They were used to receive/transmit the carrier waves from/to the Earth. The group of dipole antennas was installed on the top panel of the satellite that was aligned with the spin axis, and the X-band group of dipole antennas was connected to the top of the S-band group (Iwata

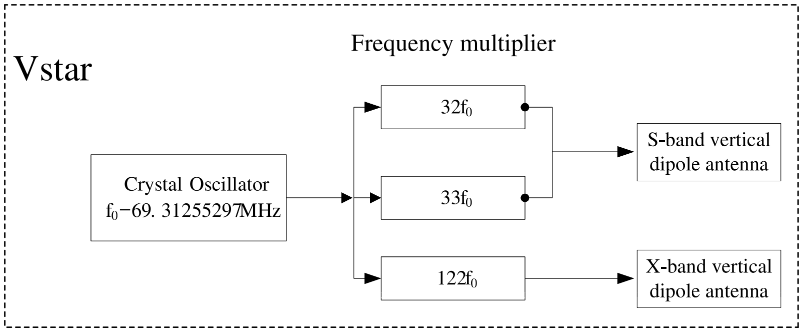

Fig. 1 S- and X-band transmitter on *Vstar*. Two S-band and one X-band carrier signals are all synchronized from the same crystal oscillator.

et al. 2001). The geometric center of the medium-gain antennas was on the axis of the satellite. For each side of the satellite, pieces of a collar and skirt were used to balance the solar radiation pressure. Nevertheless, nutation of the spin axis inevitably occurred with long-term periods. Such nutation could reduce the lifetime of the satellite, and could add modulation to the radio signal arising from the spin, when the antenna phase center was not coincident with the geometric center and the geometric axis was not coincident with the spin axis. To reduce this nutation, a circular tube that was half-filled with mercury was added to the inside of the subsatellites as a nutation dumper. The spin frequency was found to be ~ 0.18 Hz for the two subsatellites. The phase of the transmitted radio signal changed by a few tens of degrees with spin frequency and its harmonics. The effect of phase changes could be reduced by taking an average from the long-term sampled data. The narrow band phase tracking of the signal from the satellite enabled us to effectively remove such phase changes. Schematic diagrams of the S- and X-band transmitters onboard *Vstar* are shown in Figure 1. Two frequency signals in the S-band and one in the X-band were generated from the same crystal oscillator on *Vstar*, so they were synchronized and coherent.

These signals from the subsatellites were received at the ground VLBI station. A schematic diagram of the receiver system is shown in Figure 2. The VLBI system here is composed of the following parts: the front end of the telescope consists of a low-noise amplifier, a down-converter and a first local oscillator that converts the received radio wave in S/X-bands into an intermediate frequency (IF) signal with a frequency of several hundred MHz. The back end of the telescope consists of a down-converter and a second local oscillator that converts the IF signal into a video-band signal with a frequency of a few tens of kHz; the digitized narrow band recorder system of the "IP-VLBI" / SRTP-station was used in the experiment. Four video-band signals were simultaneously sampled at a rate of 200 kHz with 6 bit quantization by an analog-to-digital (A/D) converter in the SRTP-station (Ping et al. 2000; Hanada et al. 2010). The output data from the A/D converter were recorded on hard disks with integer values ranging from –32 to 31. All the reference frequencies and time signals, such as those from the down-converter and A/D sampler, were provided by an ultra stable hydrogen maser clock at each ground VLBI station.

In the *SELENE* radio science experiments, scheduled radio occultation observations were made by the Usuda deep space tracking station (Imamura et al. 2010). The final results were released in the *SELENE* database archive, as seen in the review from *http://l2db.selene.darts.isas.jaxa.jp/index.html.en*. VLBI multi-bit sampling of raw data recorded at a single site can be used to retrieve information about the lunar ionosphere as a by-product during the occultation periods.

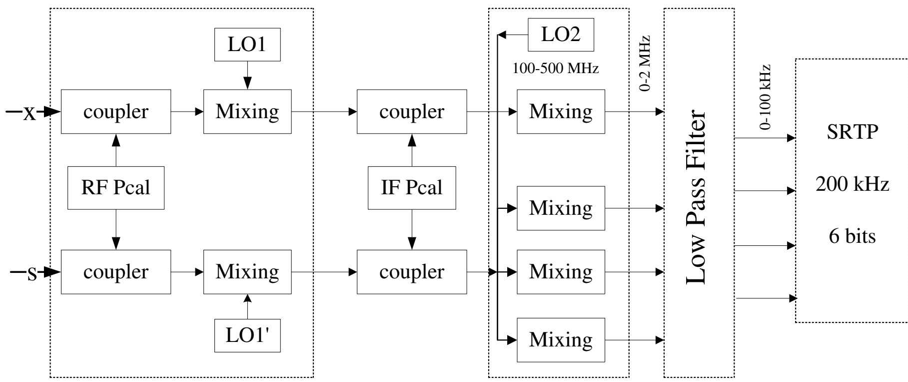

Fig. 2 Receiver system that is part of the ground station.

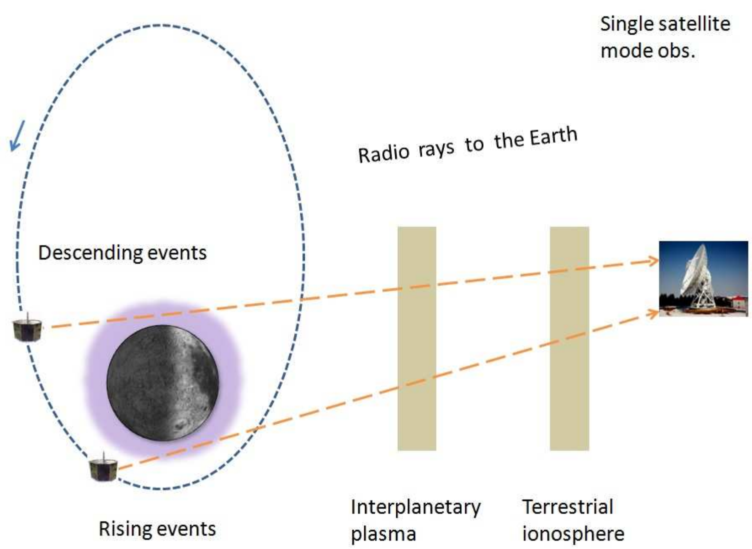

Fig. 3 How an occultation occurs.

3 PRINCIPLE OF TEC ESTIMATION BY A DUAL FREQUENCY METHOD

Ground-based radio occultation observation, which is a common technique used to investigate planetary atmospheres and ionospheres, has the advantages of high precision, high resolution, not being affected by ground weather and being economical. When a ground-based antenna tracks an orbiter near the target planet by using grazing occultation, the radio waves from the orbiter pass through the ionosphere or atmosphere, if they exist, and are affected by refraction and propagation delay. Researchers can study the characteristics of the atmosphere by using data from the the radio signal obtained at the tracking station. Lunar missions can also use this method.

Figure 3 illustrates how radio occultation with a single orbiter is performed. In the case of *Vstar*, it was sometimes occulted by the ionosphere above the lunar surface and was observed from a ground VLBI tracking station. In the observed phase shift of radio signals from *Vstar*, contributions from the terrestrial ionosphere, the interplanetary plasma, and the lunar ionosphere along the radio signal path between the satellite and the ground antenna are involved. Refraction by the terrestrial neutral atmosphere, including the troposphere and stratosphere, was one of the major sources of error in this study. Together with the instrumental error, these large errors can be removed using a geometry-free analysis method that uses dual frequencies. The influences of the terrestrial troposphere, the receiver noise and the undetermined constant errors were almost identical in the *Vstar* dual frequency radio signals, since two signals followed almost the same the propagation path. The components of the phase shift introduced by the interplanetary plasma and by the terrestrial ionosphere were removed by using the combined phases of the signals from *Vstar* just before and/or after the occultation event. The phase shift caused by the terrestrial ionosphere could be a hundred times or more larger than that by the lunar ionosphere, but still exhibit a small variation during the radio occultation period. It was necessary to observe for $50 \sim 100\,\mathrm{s}$ before or after the occultation to estimate and remove the influences of the interplanetary plasma and the terrestrial ionosphere. Usually the phase shifts introduced by the terrestrial ionosphere during the occultation were not exactly the same as those $50 \sim 100\,\mathrm{s}$ before the occultation. Thus, the component of the terrestrial ionosphere could not be perfectly removed from the total phase shift using the same simple procedure. In order to eliminate the component of the terrestrial ionosphere, considering a linear variation during $\sim 110\,\mathrm{s}$ of occultation, an efficient extrapolation algorithm was used based on the time sequence of the phase shifts. Then, the total electron content (TEC) profiles in the ionosphere of the Moon were obtained. This method was also used by Imamura et al. (2010).

Vstar that was part of the *SELENE* mission transmitted three carrier signals in the S-band and one in the X-band, which were named S8/S9/X2. They were synchronized in time and had a coherent phase at different frequencies. The nominal carrier frequencies transmitted before launch were set by Equation (1) (Iwata et al. 2001),

$$f_i = C_i \cdot (f_0 + \Delta f_0); \quad f_0 = 69.31255297\,(\mathrm{MHz})\,, \tag{1}$$

where Δf_0 was the drift of the crystal oscillator, and C_i were the scale factors, which were 32, 33 and 122 for the S8, S9 and X2 bands, respectively. The TEC of the lunar ionosphere can be estimated from the phase information of the radio waves recorded by a single ground station. Because the ionosphere is a dispersive medium, the ionospheric delay along the path of the signal is inversely proportional to the square of the radio wave's frequency. Linear combinations of the phases in two coherent frequencies allow us to extract contributions from the lunar ionosphere.

The phase information for the received signal is denoted by Equation (2),

$$\Phi_i = 2\pi f_i \tau_{\mathrm{total}} + 2\pi \cdot \frac{40.3}{c} \cdot \frac{\mathrm{TEC}}{f_i} + \Phi_i^{\mathrm{spin}} + \Phi_i^{\mathrm{const.}}\,, \tag{2}$$

where i represents the channel of the recorded coherent signal (S8, S9 and X2); f_i is the corresponding frequency; τ_{total} includes common delays in the S/X bands such as the geometric delay, the tropospheric delay, clock offset, instrumental delay and so on; c is the speed of light; Φ_i^{spin} is the phase caused by the satellite spin; and $\Phi_i^{\mathrm{const.}}$ is the mutual phase difference, which is a constant or varies slowly over a few tens of minutes.

In the *SELENE* mission, *Rstar* and *Vstar* were spin stabilized subsatellites, and for each of them the direction of the spin axis was almost perpendicular to the lunar orbital plane. However, the spin axis slightly swayed due to nutation of the satellite, and it could modulate the radio signal with the frequency of the spin and the harmonic frequencies. Additionally, the main lobe from the group of dipole antennas in the S-band was in the direction perpendicular to the axis, and the effects of interference from the top panel and the collars of the satellite were detected. These effects, however, were not significant for the group of dipole antennas in the X-band because it was higher than the top panel. Due to the motion of the satellite, periodic signals due to the spin and the nutation with higher frequency harmonics might appear in the phase of received signals and appear as a Doppler shift. The observed time series of the signal phase show modulations with a period of $\sim 5.35\,\mathrm{s}$ due to the spin of *Vstar*.

Based on the relation between the TEC and the phase differences of S8 and X2, the TEC is described by Equation (3),

$$\Delta\Phi = \Phi_{S8} - \frac{32}{122} \cdot \Phi_{X2} = 2\pi \cdot \frac{40.3}{c} \cdot \frac{\mathrm{TEC}}{f_i} \cdot \left(\frac{1}{32} - \frac{32}{122^2}\right) + \Delta\Phi^{\mathrm{spin}} + \Delta\Phi^{\mathrm{const.}} , \quad (3)$$

where $\Delta\Phi$ is the corresponding phase difference between Φ_{S_8} and Φ_{X_2}. The term $\Phi_{S_8} - \frac{32}{122} \cdot \Phi_{X_2}$ contains the phase difference between the initial phase and the phase caused by instrumental delays onboard the satellite and by the ground instruments. The TEC cannot be directly derived from Equation (3). The change in TEC from $t = 0$ to $t = t$ can be derived by Equation (4),

$$\begin{aligned} \Delta\mathrm{TEC} &= \frac{32 \cdot f_0}{\frac{122^2 - 32^2}{122^2}} \cdot \frac{1}{2\pi} \cdot \frac{c}{40.3} \cdot \frac{\pi}{180} \cdot [\Delta\Phi(t) - \Delta\Phi(0)] \\ &\approx 0.00492 \cdot [\Delta\Phi(t) - \Delta\Phi(0)] \ (\mathrm{TECU}) . \end{aligned} \quad (4)$$

TECU (total electron content unit) is equal to 1×10^{16} electrons in one square meter of air. That is, 1 TECU = 1×10^{16} element/m^2.

4 RESULT OF OBSERVATION

This section describes the results from tracking data at two VLBI stations, Iriki and Ishigaki. The effective aperture of the antennas at both stations is 20 m. The two stations are located at longitude and latitude $E130°6'$, $N31°4'$ and $E124°0'$, $N24°4'$, respectively. One ionospheric event that was observed during the ingress of the occultation, which occurred from UT 22:18 to UT 22:20 on 2008 June 28 for 108 s, was found and retrieved from the VLBI observation database. The stations at Iriki and Ishigaki received the radio waves which passed 60–30 km and 30–0 km above the lunar surface, for the periods from 22:18:00.021 to 22:18:55.006 (about 55″) and from 22:18:55.006 to 22:19:48.745 (53″), respectively. These data were processed and methodically analyzed to extract the TEC of the lunar ionosphere along the signal paths. During the occultation period, the tangent point of the occultation projected on the surface of the Moon was at an East longitude of $\sim E62.5°$ and a North latitude of $\sim N73.4°$, with a solar zenith angle of $\sim 104°$.

Phase shifts due to the Doppler effect were extracted from radio waves in a one-way link between *Vstar* and a VLBI station. The flow chart showing the data processing method is given in Figure 4. The signals intercepted by the radio telescope in the VLBI station were recorded and stored in a hard disk as binary data, which we converted to floating point values for processing. Random noise was first eliminated from the data. In the 1st Fast Fourier Transform (1st FFT), we find the maximum power by the centroid method using 65 536 sampled data as one interval unit in the FFT. Then the reference frequency signal is constructed in each FFT unit. The frequency corresponding to the spectral peak is used for estimating the phase rotation in a later process. The band-pass filter is used in the frequency domain to extract the signal in the 1st inverse FFT. The target signal is compared with the reference signal in the frequency domain and rotated in the time domain, then it is low-pass filtered in the frequency domain. Then the 2nd FFT and the low-pass filter are applied to the target signal to get the low frequency signal in the frequency domain. After the 2nd inverse FFT, the 4096 phase data of the real part and the imaginary part are obtained separately for each interval. Every 4096 data are accumulated and 16 data sets of real and imaginary parts are obtained in one FFT unit. After correction for the phase slip in an FFT unit, the time series formed by the observed phase of the target is obtained. The results from the above processes for the X2-band signal are illustrated in Figure 5(a)–(f).

The total phase differences calculated from the S8/X2-bands are shown in Figure 6(a) using black dots, with the trend component and the residual phase using red circles and blue dots, respectively. The spectra of the phase difference and the spectra after removal of the effect due to spin

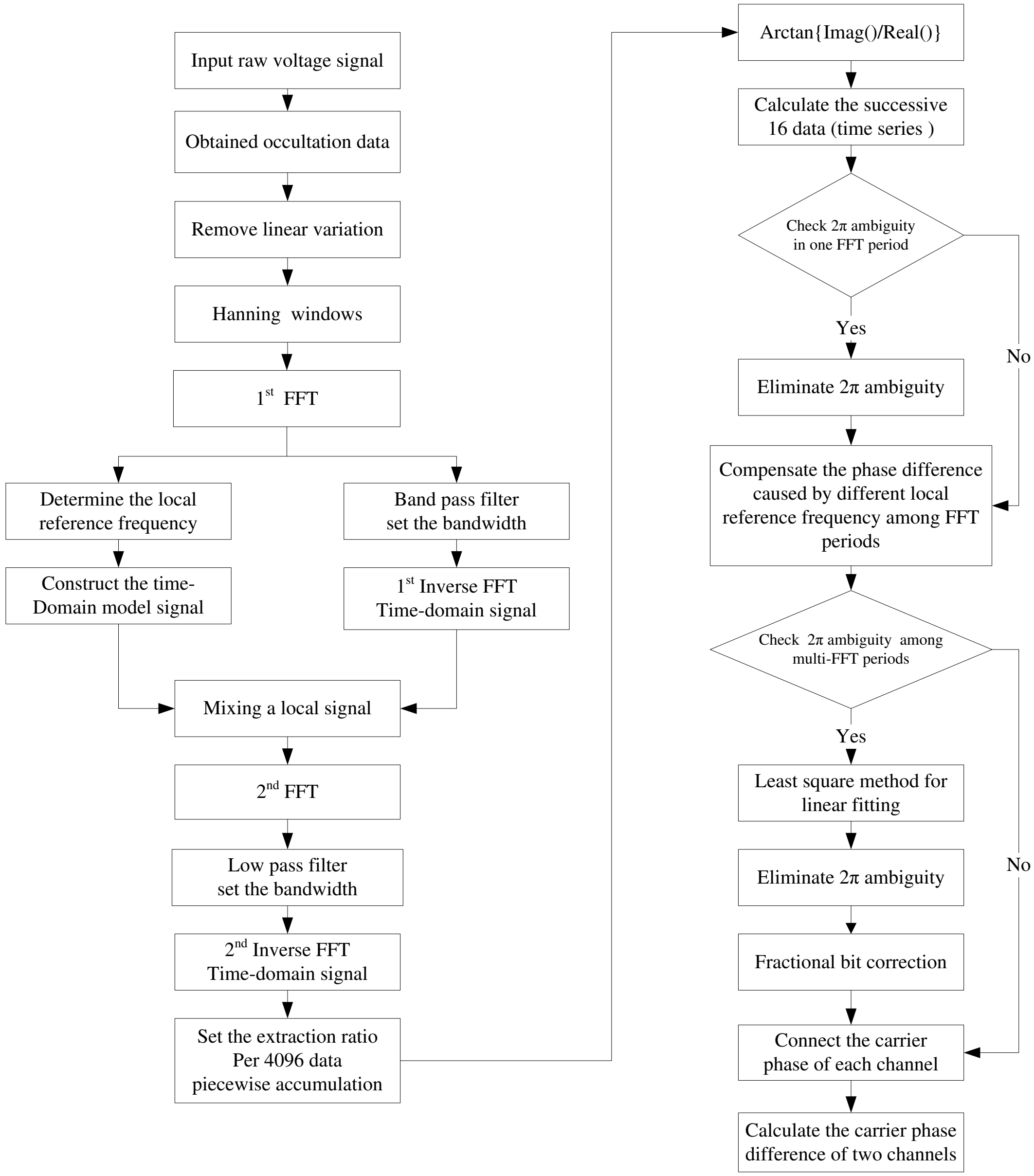

Fig. 4 A flowchart showing the process of phase extraction.

using a low pass filter are shown in the upper and the lower panels of Figure 6(b), respectively. Then the phase variations, after removal of the effect of the spin, are obtained and shown in Figure 6(c) using black dots, where the trend is not compensated. Finally, we get the phase variation, including the compensated trend, and that processed by Gaussian smoothing as shown in Figure 6(d) using a black line and red line, respectively.

In the conventional single-satellite occultation method, the additional influences caused by the terrestrial ionosphere and interplanetary plasma along the signal path could not be eliminated thoroughly. We follow the idea in Imamura et al. (2010) and Imamura et al. (2012) that the total TEC

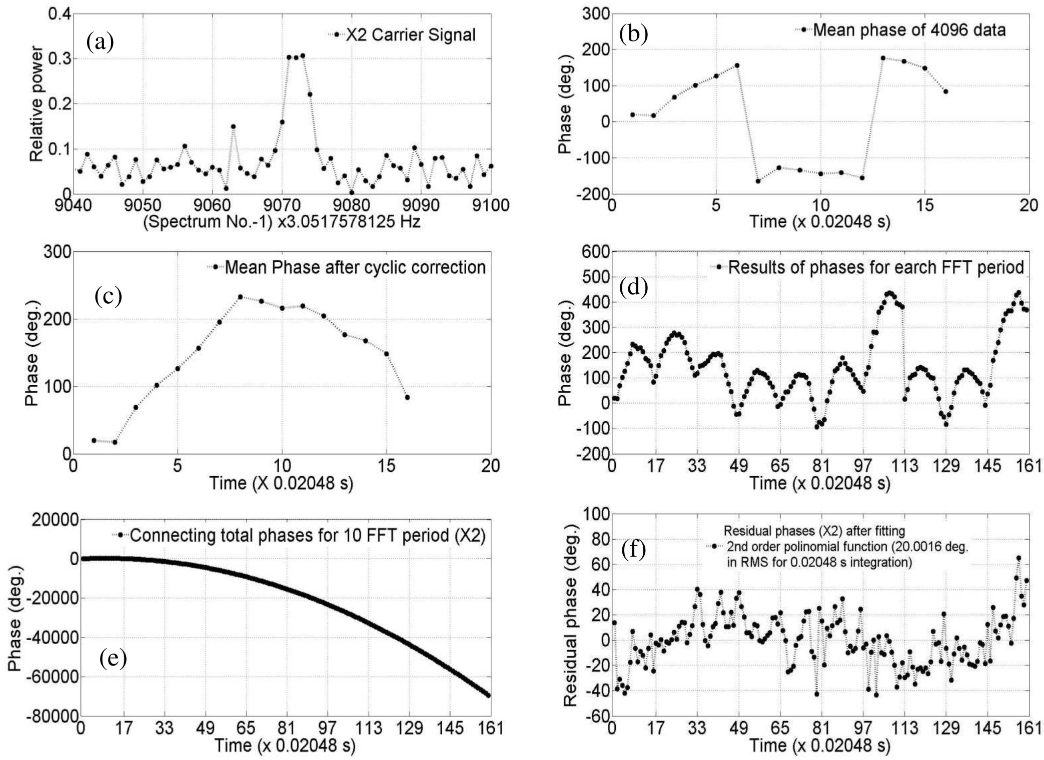

Fig. 5 (a) The X2-band carrier signal; (b) before cyclic correction, the 4096 phases average into one phase, which forms 16 data in one interval unit of FFT; (c) after cyclic correction, 16 data are in in one FFT unit; (d) before cyclic correction between two neighboring integrated time intervals, the phases are in 10 FFT units; (e) after cyclic correction, the phases are in 10 FFT units; (f) after fitting a second order polynomial function, the standard deviation of the residual phases of the X2-band is 20.0016 degrees for a 0.02048 s integration. The "cyclic correction" is the correction of integer ambiguity or that of the cycle slips of the combined carrier phase. There are two kinds of phase cycle slips: (1) the possible phase slips between two neighboring integrated time intervals; (2) the possible phase slips in a given integrated time.

contains the terrestrial ionosphere and interplanetary plasma in the range from 60 to 30 km above the lunar surface, and that the terrestrial ionosphere and interplanetary plasma along the signal path are constant or linear, varying during the time of occultation by about 110 s. These components can be removed from the TEC by means of linear fitting of the data obtained before and/or after the occultation, when the signal is not affected by the lunar ionosphere. The TEC profile during 110 s of the total occultation interval for 0 to 60 km above the lunar surface is shown in Figure 7 as a cyan line. According to the statistical results of the *SELENE* mission, the lunar ionosphere higher than 30 km above the lunar surface is too thin to be considered. We assume that above 30 km, interplanetary plasma dominates the lunar ionosphere, so we truncate the lunar ionosphere at 30 km. This is a fixed point for fitting effects of the interplanetary plasma and terrestrial ionosphere. The fixed point, which is about 30 km above the surface of the Moon at 55 s after the start of ingress as shown on the horizontal axis, is indicated by a red dot. The estimated variation in TEC from 0 to 60 km is shown in Figure 7 as a magenta line for 110 s. Linear fitting of the TEC for the range higher than 30 km, which corresponds to the time from 0 to 55 s, is shown in Figure 7 as a blue line. The green line is

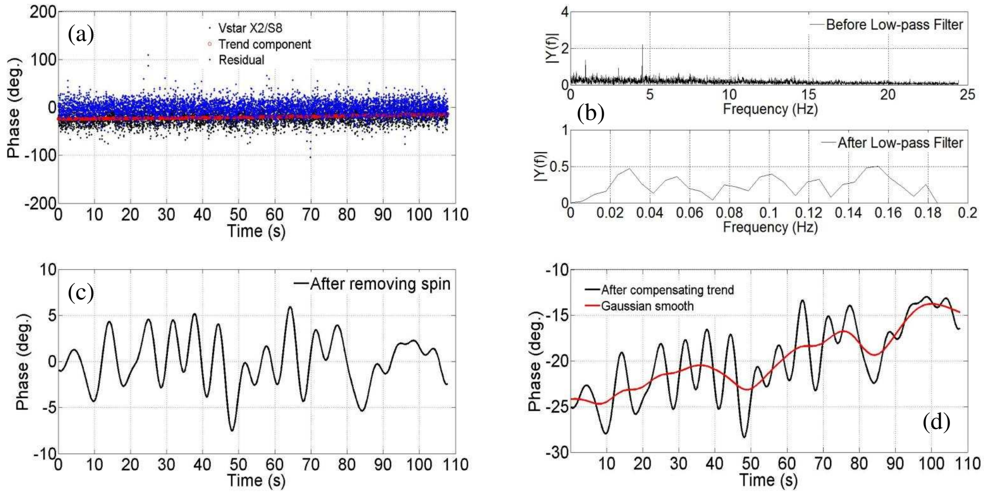

Fig. 6 (a) A time series of the differential phases, taken during the ingress of the occultation on 2008 June 28. The phase information corresponds to the satellite hidden behind the Moon as seen from the Iriki tracking station; (b) the spectrum after satellite spin is removed; (c) the phase variation for S8/X2 after satellite spin is removed; (d) the phase variation for S8/X2 after the compensating trend is added.

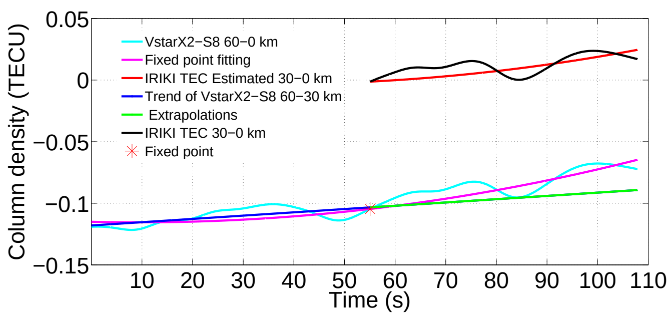

Fig. 7 The time series with variations in column density.

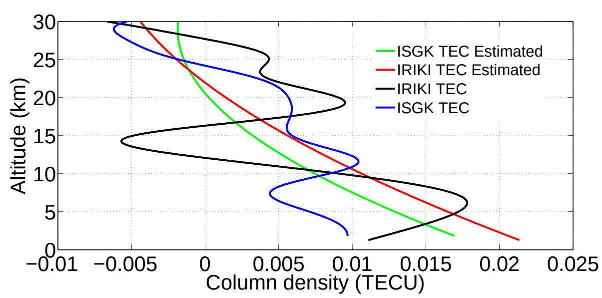

Fig. 8 The electron column density profiles in the ionosphere of the Moon.

a simple extension of the blue line for interplanetary plasma and terrestrial ionospheric TEC below 30 km. The green line is slightly different from the trend of the TEC for lower than 30 km, as shown in Figure 7 from 55 to 110 s. Finally, the TEC in the lunar ionosphere is obtained from the data for about 53 s by subtracting the green line from the cyan line, as shown in Figure 7 using a black line. The trend that results by subtracting the green line from the magenta line is also shown in Figure 7 using a red line. The S8 and X2-band residual phases for an integration of 0.02 s after fitting a second degree polynomial is 13.3 and 20.0 degrees, respectively, which corresponds to about 0.19 and 0.28 degrees in RMS for a 100 s integration, respectively. The error that comes from the difference in the phases between the S8 and X2 bands for a 100 s integration in RMS is obtained according to Equation (5),

$$\sqrt{\frac{\text{Integration time}}{\text{Occultation time interval}}} \times \sqrt{\text{RMS}_1{}^2 + \text{RMS}_2{}^2}$$
$$= \sqrt{\frac{0.02}{100}} \times \sqrt{13.3^2 + (20 \times \frac{32}{122})^2} \approx 0.2^\circ \,, \tag{5}$$

where RMS1 and RMS2 correspond to the Root Mean Square for Integration time. The resolution of the total phase is 0.2 degrees and the theoretical resolution of TEC becomes 0.001 TECU corresponding to this phase resolution. This means that the VLBI observation has a sensitivity better than $\sim 10^{14}$ m^{-2} for the TEC in the range from 0 to 30 km above the lunar surface.

In Figure 8, the vertical profile of the TEC along the signal path is converted from the time series data. The vertical axis here is the height of the tangent point of the occultation path near the Moon's surface. The variation in TEC observed from the Iriki VLBI station is shown by the black line and its trend is shown by the red line. For comparison, the TEC observed from the Ishigaki VLBI station, which was estimated using the same method as above, is also shown by the blue line with the trend of the green line. As seen from Figure 8, the difference between the results of the lunar ionosphere from Iriki and Ishigaki is less than 20% compared to the TEC trend. However, these results are about 30% or ~ 0.01 TECU weaker than the result observed at the Usuda station, as released in the *SELENE* database archive, and weaker than the results given by Ando et al. (2012).

5 DISCUSSION AND CONCLUSIONS

Some cases of lunar occultation data were found in a large amount of VLBI tracking data acquired during the *SELENE* mission. We analyzed the *Vstar* occultation data to retrieve the lunar ionosphere as a useful by-product. The differential carrier phases of the coherent S/X band signals have been used to calculate the lunar ionospheric electron contents. In the data analysis, we removed the contribution from the terrestrial ionosphere, and derived the effect of the lunar ionosphere from the VLBI data. Observations at different ground sites that were ~ 1000 km apart gave identical results. The independent observations and data processing methods enhanced the reliability of the results. The Usuda tracking station obtained a TEC of ~ 0.03 TECU in the bottom layer for the same event; the TEC results have been released in the *SELENE* data archive. This result is $\sim 30\%$ higher than results collected from multiple sites that were obtained in this paper. This may indicate that the Moon has a weaker and thinner ionosphere than what was estimated before. There were only a few cases of occultation in the *SELENE* VLBI observations. We are trying to use more data for this kind of study to compare the results from different sites. This kind of difference should be studied in detail in future missions. The method developed here can also be implemented in a study of planetary ionospheres. The question of whether a relatively weaker lunar surface ionosphere exists is still unresolved. Exploring the lunar ionospheric density will need other independent techniques, like active and/or passive radar observations that are part of future missions on the lunar surface that can observe at kilometer wavelengths.

Acknowledgements The authors thank the *SELENE* Project for conducting these VLBI experiments and producing data for the community. The data used in this paper were acquired under a cooperation framework between NAOJ/NINS and XAO/CAS. The authors are grateful for discussions with Prof. Nobuyuki Kawano on data analysis and thank Prof. Qinghui Liu for the fruitful assistance on this work. We also thank Prof. K. Matsumoto for discussions on the attitude of *Vstar* in orbit.

References

Ando, H., Imamura, T., Nabatov, A., et al. 2012, Journal of Geophysical Research (Space Physics), 117, 8313

Andrew, B. H., Branson, N. J. B. A., & Wills, D. 1964, Nature, 203, 171

Bauer, S. 1996, Limits to a lunar ionosphere, Anzeiger Abt II, 133, 17

Daily, W. D., Barker, W. A., Parkin, C. W., Clark, M., & Dyal, P. 1977, J. Geophys. Res., 82, 5441

Hanada, H., Iwata, T., Liu, Q., et al. 2010, Space Sci. Rev., 154, 123

Imamura, T., Iwata, T., Yamamoto, Z.-I., et al. 2010, Space Sci. Rev., 154, 305

Imamura, T., Nabatov, A., Mochizuki, N., et al. 2012, Journal of Geophysical Research (Space Physics), 117, 6303

Iwata, T., Takahashi, M., Namiki, N., et al. 2001, Journal of the Geodetic Society of Japan, 47, 558

Kobayashi, H., Sasao, T., Kawaguchi, N., et al. 2003, in Astronomical Society of the Pacific Conference Series, 306, New technologies in VLBI, ed. Y. C. Minh, 48

Liu, Q., Kikuchi, F., Matsumoto, K., et al. 2010, Radio Science, 45, 2004

Namiki, N., Iwata, T., Matsumoto, K., et al. 2009, Science, 323, 900

Ping, J., Kono, Y., Tsuchiya, A., & Kawano, N. 2000, Journal of the Geodetic Society of Japan, 46, 187

Savich, N. A. 1976, Cislunar plasma model, in Space research XVI, ed. M. J. Rycroft, 941

Schlüter, W., Himwich, E., Nothnagel, A., Vandenberg, N., & Whitney, A. 2002, Advances in Space Research, 30, 145

Stern, S. A. 1999, Reviews of Geophysics, 37, 453

Stubbs, T. J., Glenar, D. A., Farrell, W. M., et al. 2011, Planet. Space Sci., 59, 1659

Vasil'Ev, M. B., Vinogradov, V. A., Vyshlov, A. S., et al. 1974, Cosmic Research, 12, 102

Vyshlov, A. S. 1976, Space Research XVI, ed. M. J. Rycroft, 945

Vyshlov, A. S., Savich, N. A., Vasilyev, M. B., et al. 1976, NASA Special Publication, 397, 81

Vyshlov, A. S., & Savich, N. A. 1979, Cosmic Research, 16, 450

Walbridge, E. 1973, J. Geophys. Res., 78, 3668